Needle dynamics modelling and control in prostate brachytherapy

Article *in* IET Control Theory and Applications · July 2012

DOI: 10.1049/iet-cta.2011.0449

2 authors:

Arash Maghsoudi
Islamic Azad University Tehran Science and Research Branch
15 PUBLICATIONS **281** CITATIONS
SEE PROFILE

Mehran Jahed
Sharif University of Technology
67 PUBLICATIONS **603** CITATIONS
SEE PROFILE

Published in IET Control Theory and Applications
Received on 22nd July 2011
Revised on 25th December 2011
doi: 10.1049/iet-cta.2011.0449

ISSN 1751-8644

Needle dynamics modelling and control in prostate brachytherapy

A. Maghsoudi[1] *M. Jahed*[2]

[1]*Robotics and Machine Vision Lab, School of Electrical Engineering, Sharif University of Technology, Tehran, Iran*
[2]*School of Electrical Engineering, Sharif University of Technology, Tehran, Iran*
E-mail: a_maghsoudi@ee.sharif.ir

Abstract: Although 'Needle steering' is considered a challenge in needle insertion strategies, needle control becomes a crucial training tool for evaluating surgeon's skills in such critical incision. In this study, a model-based dynamics equation for the needle movement through the soft tissue is developed. In the proposed control scheme, the force estimation calculated through the simulated tissue deformation data and the dynamic finite element as the tissue model, is used as the force feedback. To point out the role of mechanical properties of the soft tissue, an inverse dynamics control method is used to demonstrate the system performance in presence of uncertainty in tissue mechanical parameters. Moreover, it is shown that the uncertainty in the tissue mechanical parameters dramatically affects the system performance as well as causing instability. Hence subsequently, a robust control approach is designed to compensate for the undesirable effect of parameter uncertainty in the system.

1 Introduction

Needle insertion is an inevitable part of many modern medical procedures. In all of these procedures a target deep inside the anisotropic, visco-elastic, inhomogeneous and multi-layered soft tissue must be reached via inserting needles. Procedures such as brachytherapy [1], biopsy [2] and neurosurgery [3] require accurate needle insertion techniques.

In Prostate Brachytherapy and following prostate tissue biopsy, the physician delivers the radioactive seeds such as ^{103}Pd in the predetermined targets by a needle inserted into the prostate. Often the physician uses the trans rectal ultrasound images to guide the needle. Owing to the vicinity of the vital organs such as bladder, the inaccurate insertion and misplacement of the radioactive seeds may lead to severe trauma.

The accuracy of the needle insertion is adversely affected by a number of factors. A needle, frequently assumed to be flexible, is inserted into a soft tissue induces complex mechanical interactions and may result in considerable uncertainties. Tissue intrinsic characteristics as well as its deformation and rotation may cause dramatic complexities. Also consideration of the needle flexibility and its tip structure may contribute to further complexities (for a survey of related studies see [4]).

In addition to the mentioned issues, human error factors and physician exhaustion as a result of repeated attempts to guide the needle in procedures such as prostate brachytherapy, justify the study of needle control procedures.

Modelling soft tissue behaviour seems to be crucial in simulation studies of the needle insertion procedure and specifically, in the current approach of controlling the needle through a model-based scheme. Finite-element model (FEM) as a powerful solution to solid mechanics problems has been widely used for the simulation of the soft tissue behaviour [5]. DiMaio and Salcudean [6] used a two-dimensional (2D), static and linear FEM model to represent a linearly elastic soft tissue. Alterovitz *et al.* [7] used a dynamic and linear FEM to model the soft tissue and thereby considered the mass of each element and velocity-dependent forces in the FEM formulation. Goksel *et al.* [8, 9] used a 3D FEM model of the prostate for the simulation of the prostate brachytherapy. Dehghan and Solcudean [10] simulated the prostate with a 3D FEM with the Neo–Hookean constitutive equation; however, they used their more complex model only in simulation and their experimental results utilised the linear FEM because of the considerations of real-time implementation.

Many researchers have investigated the interaction between needle and the tissue [11–15]. Maurin *et al.* [11] studied the forces involved during *in vivo* needle insertion in liver and kidney. Simone and Okamura [12] measured the forces involved during needle insertion in bovine liver and tried to model the forces by dividing the measured force into cutting forces, friction forces (using Karnopp stick-slip model [16]) and stiffness forces. DiMaio and Salcudean [17] estimated the force distribution along needle using a homogenous and Hookean 2D tissue phantom. By measuring the phantom deformation and using the FEM model of the phantom, they calculated the force distribution, thereby suggesting two categories of forces: friction along the needle shaft and cutting at the needle tip. They also reported that the shaft force is velocity dependent whereas the tip force remains somewhat constant for different

velocities. Crouch *et al.* [18] proposed a velocity-dependent force model for needle insertion based on the force measured while inserting needle into a tissue phantom at different velocities. Their model does not include the dependency of the forces of soft tissue mechanical properties. Dehghan *et al.* [19] developed an algorithm to find the distribution of the force along the needle shaft using the ultrasonic tissue deformation data taken from a prostate phantom. Their force model had three parameters: the force along the shaft, the tip force and the width of the tip force.

Since non-holonomic constraints govern the kinematics of the needle in the tissue, many researchers have focused on the subject of 'needle steering'. DiMaio and Salcudean [20] introduced a Jacobian matrix that defines the relationship between the needle tip and the needle base velocity. They used a potential field algorithm for motion planning of the needle tip while avoiding the obstacles in the tissue. They used the Jacobian matrix to find the desired motion of the needle base; however owing to the complexity of needle–tissue interaction and absence of a closed-form for the Jacobian matrix, it was determined experimentally through insertion of the needle in homogenous and isotropic PVC.

Alterovitz *et al.* [21] steered a bevel-tip needle inside a 2D tissue model under Markov uncertainty. Alterovitz *et al.* [22] optimised the insertion point of the needle using a search-based algorithm. They found the optimal depth by simulation of the needle at a given insertion height and chose the depth with minimum error. To find the optimal height they used a golden section search. Alterovitz *et al.* [23] also found the optimal insertion point and angle for a flexible needle while avoiding the obstacles in the tissue. To solve the optimisation problem they used a penalty method in conjunction with gradient descent algorithm. Since their cost function was not directly differentiable, they used a perturbation method to find the approximation of the cost function differentiation.

Webster *et al.* [24] developed and experimentally validated a non-holonomic model for a highly flexible bevel-tip needle. Park *et al.* [25] used the diffusion-based motion planning while considering the non-holonomic kinematics constraints for a highly flexible needle; however, they ignored the tissue deformation owing to the high flexibility of the needle. Glozman and Sohom [26] used the inverse kinematics of a flexible needle. They simulated the visco-elastic tissue with a linear beam supported by virtual springs. Dehghan and Salcudean [27] optimised the insertion point, angle and depth in a 3D tissue model for multiple targets inside the tissue. They used iterative simulation and found the best fitting line crossing all the targets in each iteration. They proved by simulation that their algorithm is converging to the optimum insertion point, angle and depth. However noticeably, none of the mentioned studies considered the tissue model parameters in their analytical and modelling efforts.

A major challenge in needle insertion procedures is the soft tissue mechanical parameters estimation. To point out the importance of it, a few researchers have done the sensitivity analysis of the target-reaching error with respect to tissue parameters. DiMaio and Salcudea [17] examined the sensitivity to Young modulus in his simulation studies. Alterovitz *et al.* [7] simulated the sensitivity analysis for the Young modulus in addition to other insertion parameters such as insertion point, velocity and needle sharpness. They proposed that an increase in the Young modulus value decreases the error whereas changes in the Poisson ratio do not affect the error at all. To provide a more realistic model for prostate brachytherapy, Maghsoudi *et al.* [28] considered the anatomical constraint on the prostate.

Table 1 Prostate stiffness (in kPa) in normal and abnormal tissues *in vitro* [29]

	2% pre-compression		
strain rate (per second)	0.4%	4%	16%
normal anterior ($n = 32$)	55 ± 14	62 ± 17	59 ± 19
normal posterior ($n = 32$)	62 ± 19	69 ± 17	65 ± 18
BPH ($n = 21$)	38 ± 8	36 ± 9	38 ± 8
CA ($n = 28$)	96 ± 19	100 ± 20	99 ± 18

Ophir *et al.* [29] used the ultrasonic elastography method to measure the soft tissue mechanical properties. Their studies showed that for the prostate, the Young modulus differs considerably between the normal, benign prostatic hyperplasia and prostatic carcinoma (CA) (see Table 1).

To improve the accuracy of the needle insertion, previous efforts were mostly focused on tissue modelling, needle steering and needle–tissue interaction. However, the problems addressed in this paper are the needle 'dynamics' and the needle 'control'. The goal of this study is to define the needle insertion problem in the realm of dynamics while introducing a novel method for the estimation of the force, based on the finite-element method. The proposed dynamics model relies on the model-based needle–tissue interaction forces and uses simulated tissue deformation data to estimate the force. The undesirable effect of the parameter uncertainty is shown through usage of inverse dynamics control method and finally a robust control law is proposed to achieve robustness under uncertainty in the model parameters. The paper is organised as follows: section 2 provides a description of the methods used in this paper including tissue model, needle–tissue system, FEM-based force estimation and needle control. Section 3 presents the simulation results followed by discussion and conclusion in Sections 4 and 5, respectively.

2 Methods

2.1 Dynamic finite-element modelling of tissue

In general, linear static problems in elasticity require solving the following three equations [30]

$$\begin{aligned} \varepsilon &= \frac{1}{2}(\nabla w + (\nabla w)^{\mathrm{T}}) \\ \nabla \cdot \sigma^{\mathrm{T}} + F &= 0 \\ \sigma &= 2\mu\varepsilon + \lambda(\mathrm{tr}(\varepsilon))I \end{aligned} \tag{1}$$

where w is the displacement vector field, ε is the strain tensor field, σ is the stress tensor field, μ and λ are the Lamé material constants, I is the identity matrix, $\mathrm{tr}(\cdot)$ denotes the trace of matrix and F is the field of the body force per unit volume.

Solutions to the equations of elasticity can be established in terms of either finding a displacement field w that satisfies the Lamé–Navier equations or finding a stress field that

doi: 10.1049/iet-cta.2011.0449

satisfies the equations of equilibrium and the Beltrami–Michell compatibility equations [31].

The Lamé–Navier equations can be written as

$$(\lambda + \mu)\nabla(\nabla \cdot w) + \mu\nabla^2 w + F = 0 \tag{2}$$

However, in dynamic problems of elasticity, the Lamé–Navier equation can be written as [32]

$$(\lambda + \mu)\nabla(\nabla \cdot w) + \mu\nabla^2 w + F = \rho\frac{\partial^2 w}{\partial t^2} + \xi\frac{\partial w}{\partial t} \tag{3}$$

where ρ is the density of the material and ξ is the damping constant of the material.

The solution of (3) using FEM [32] results in the following equation

$$M\ddot{\hat{w}} + C\dot{\hat{w}} + K\hat{w} = F \tag{4}$$

where M is the system mass matrix, C is the system damping matrix, K is the global stiffness matrix and $\hat{w}$ represent the values of w in the discrete space.

Determination of the damping matrix C is difficult practically since it requires the knowledge of the viscous parameter (ξ). It is often assumed, that the damping matrix is a linear combination of mass and stiffness matrices [33]

$$C = \alpha K + \beta M \tag{5}$$

where the parameters α and β are determined experimentally. Such damping is known as the 'Rayleigh damping'.

2.2 Needle–tissue system description

Fig. 1 considers a conventional configuration of a needle insertion procedure into the soft tissue. The ultimate goal is to steer and control the needle to reach a target located deep inside the prostate. As seen in the ultrasonic images, the prostate is constrained by the pubic bone, which is the source of the rotation of prostate tissue during needle insertion.

The forces applied to the needle can be divided into two categories: the control signal that is applied on the base of the needle and the distributed force on the needle shaft, applied by the tissue. So considering a prismatic movement of a rigid needle, the dynamics equation of the system

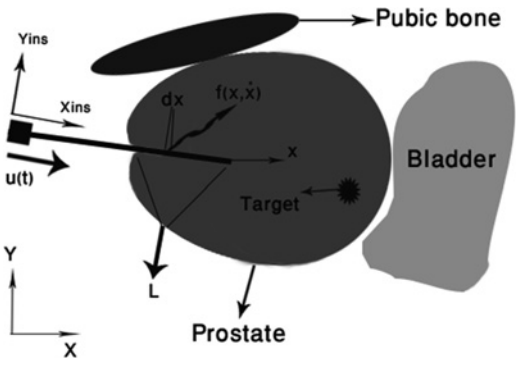

Fig. 1 *Conventional needle insertion configuration and anatomical position of prostate*

according to Newton's second law of motion in the insertion frame $(Y_{\text{ins}} - X_{\text{ins}})$ can be written as follows

$$M_{\text{n}}\ddot{x} + \text{sign}(\dot{x})\int_0^L \vec{v}^{\text{T}} \cdot f(x,\dot{x})\,\text{d}x = u(t) \tag{6}$$

where x is the needle tip position in the insertion frame $(Y_{\text{ins}} - X_{\text{ins}})$, M_{n} is the needle mass, $f(x,\dot{x})$ is the force per length applied by the tissue to the needle at dx (Fig. 1) as a function of the needle position (x) and velocity $(\dot{x})$ [18] whereas the sign function preserves the alignment of the needle direction and the force applied to it; and L is the penetrated length of the needle into the tissue. Furthermore, $\vec{v}$ is the unit vector along the direction of the insertion projecting the force along the needle shaft and $u(t)$ is the force applied to the base of the needle in order to insert the needle into the tissue namely, the 'control law'.

2.3 Model-based force estimation for needle insertion

There are a few approaches for measuring the force that tissue applies to the needle. One may exploit the force sensor to measure the applied force while being wary of the calibration and noise issues. Other indirect methods such as force observer are proposed to estimate the force applied to the needle by measuring the velocity and position of the needle [34–36]. Although observers such as disturbance observer seems to be quite efficient in force estimation (especially owing to its simplicity for implementation), the derivation of the robust control law still requires the knowledge of the upper bound on uncertainties and the model of the system. Besides, the force estimation approach presented here can easily be used for other control approaches such as adaptive controller and robust adaptive controller.

In this work a model-based method is used for estimation of the applied force to the needle. This is due to the fact that tissue deformation and applied external force to the tissue are related as governed by tissue models such as FEM. Thereby tissue deformation may be utilised to estimate the applied external force and vice versa. The advantage of this method is that in addition to estimation of the distribution of the forces along the needle shaft, this model-based force-measuring method can be exploited in the inverse dynamics controller.

As a geometrically discrete model of the tissue is used in the context of FEM considering dynamic elasticity, the integral over the needle length can be substituted with summation of the forces applied to the needle by the nodes of the soft tissue mesh and (6) can be written as

$$M_{\text{n}}\ddot{x} + \text{sign}(\dot{x})\sum_{a=1}^{n(x)} \vec{v}^{\text{T}} \cdot \overrightarrow{f_a}(w,\dot{w},\ddot{w},\Theta) = u(t) \tag{7}$$

where $\overrightarrow{f_a}(w,\dot{w},\ddot{w},\Theta)$ is the force applied by the ath node of the soft tissue mesh, which is in contact with the needle and owing to the usage of dynamic FEM for tissue, it is a function of tissue parameters and the tissue deformation (w) and its first and second time derivatives $(\dot{w},\ddot{w})$, $n(x)$ is the number of tissue nodes in contact with the needle and it is a function of the x (i.e. the number of contact nodes increases as needle is inserted deeper into the tissue); and Θ includes the parameters of the tissue. Note that w is implicitly a function of needle velocity; because different

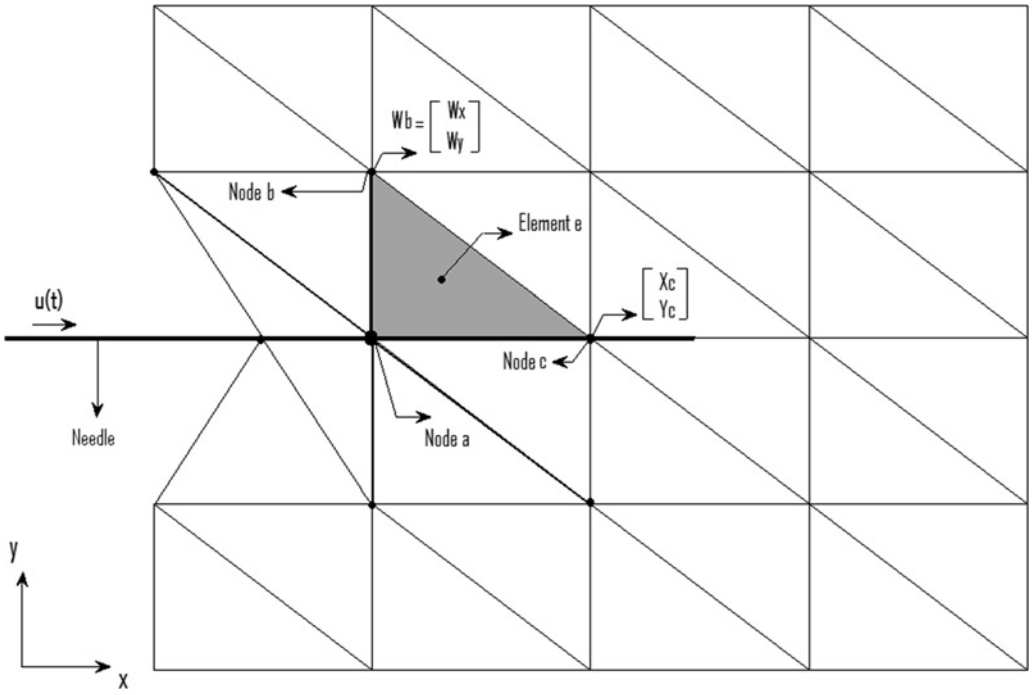

Fig. 2 *Realisation of (8)*

The force applied to the needle at node a depends on the displacement vector of the adjacent node (w_b). The coordinate of the nodes are: node a, $[X_a\ Y_a]^{\mathrm{T}}$, node b, $[X_b\ Y_b]^{\mathrm{T}}$, node c, $[X_c\ Y_c]^{\mathrm{T}}$ and the displacement vectors of the nodes are: w_a for node a, w_b for node b and w_c for node c

velocities causes different forces applied to the tissue; thus resulting in different tissue deformation [18].

In the case of the 2D and dynamic FEM for the tissue, the force applied to each contact node becomes [32]

$$\vec{f}_a(w,\dot{w},\ddot{w},\Theta)=\sum_{b=1}^{l(a)}\vec{v}^{\mathrm{T}},(M_{ab}(\Theta)\ddot{w}_b+C_{ab}(\Theta)\dot{w}_b+K_{ab}(\Theta)w_b),$$
$$w_b=\begin{bmatrix}w_{x_b}\\ w_{y_b}\end{bmatrix} \tag{8}$$

where $M_{ab}(\Theta)$, $C_{ab}(\Theta)$ and $K_{ab}(\Theta)$ are, respectively, the element mass matrix, element damping matrix and the local stiffness matrix defined between node a (in contact with the needle) and node b (connected to node a in the tissue mesh which includes a itself) and are a function of the parameters (Θ), $l(a)$ is the number of the nodes connected to the node a, w_b is the displacement vector of the adjacent node which consists of w_{x_b} and w_{y_b} that are the displacement of the node b in the x- and y-direction (see Fig. 2).

The element mass matrix for a triangular element can be written as [32]

$$M_{ab}=\frac{m}{3}\begin{bmatrix}1&0\\0&1\end{bmatrix} \tag{9}$$

where m is the mass of each element.

The local stiffness matrix for a triangular element can be written as [32]

$$K_{ab}=\frac{t}{4\Delta}*B^{T}(a)*D*B(b);\quad B(a)=\begin{bmatrix}\alpha_a&0&\beta_a\\0&\beta_a&\alpha_a\end{bmatrix}$$
$$D=\begin{bmatrix}\lambda+2\mu&\lambda&0\\ \lambda&\lambda+2\mu&0\\ 0&0&\mu\end{bmatrix}$$

$$\alpha_a=Y_b-Y_c,\quad \alpha_b=Y_c-Y_a$$
$$\beta_a=X_b-X_c,\quad \beta_b=X_c-X_a$$
$$\lambda=\frac{E\upsilon}{(1-\upsilon^2)},\quad \mu=\frac{E(1-\upsilon)}{2(1-\upsilon^2)} \tag{10}$$

where t is the thickness of the tissue, Δ is the area of each triangular element of the tissue mesh, E is the Young modulus, υ is the Poisson ratio, λ and μ are the Lamé parameters, α_a, α_b, β_a and β_b are functions of the position of the element's nodes of which node a is a part (e.g. referring to Fig. 2, node a is a part of the mesh element e). Here X_a, X_b and X_c are the x-coordinates and Y_a, Y_b and Y_c are the y-coordinates of element e in the world frame of $X-Y$ for nodes a, b and c, respectively.

The needle dynamics can now be written as

$$M_{\mathrm{n}}\ddot{x}+\mathrm{sign}(\dot{x})\sum_{a=1}^{n(x)}\sum_{b=1}^{l(a)}\vec{v}^{\mathrm{T}}\cdot(M_{ab}\ddot{w}_b$$
$$+C_{ab}\dot{w}_b+K_{ab}w_b)=u(t) \tag{11}$$

To derive the desired control rule and for stability and parameter mismatch analysis, it is preferred to linearly parameterise the external force term with respect to the parameters (Θ).

If Θ denotes the unknown tissue parameters (if Rayleigh damping is used) as

$$\Theta=[\lambda\ \ \mu\ \ \alpha\lambda\ \ \alpha\mu\ \ m\ \ \beta m]^{\mathrm{T}} \tag{12}$$

by using (10) the double summation in (11) can be parameterised with respect to Θ as

doi: 10.1049/iet-cta.2011.0449

where $y_{ab}(w_b, \dot{w}, \ddot{w})$ is a function of the tissue deformation and the position of the mesh nodes; and $\varphi(x, \dot{x}, w, \dot{w}, \ddot{w})$ is equivalent for the double summation in (13) (see (13)).

Finally by denoting $\varphi(x, \dot{x}, w, \dot{w}, \ddot{w})\Theta$ along the $\vec{v}$ (insertion direction) as $\varphi_v(x, \dot{x}, w, \dot{w}, \ddot{w})\Theta$, the needle movement dynamics equation becomes

$$M_n\ddot{x} + \varphi_v(x, \dot{x}, w, \dot{w}, \ddot{w})\Theta = u(t) \tag{14}$$

2.4 Inverse dynamics

In order to obtain the control law, the above non-linear differential equation is converted to the state-space representation.

$$\begin{aligned}(x_1 = x, x_2 = \dot{x})\\ \dot{\chi} = \begin{bmatrix}\dot{x}_1\\ \dot{x}_2\end{bmatrix} &= f(\chi, t) + Bu(t)\\ &= \begin{bmatrix} x_2 \\ -\dfrac{\varphi_v(x_1, x_2, w, \dot{w}, \ddot{w})\Theta}{M_n}\end{bmatrix} + \begin{bmatrix}0\\ \dfrac{1}{M_n}\end{bmatrix} u(t)\end{aligned} \tag{15}$$

Next, the standard design procedure of the sliding mode control to derive the control law is followed [37].

First a switching manifold is selected which becomes an attractor in the sliding-mode phase. The manifold is chosen as

$$s = x_2 + (x_1 - x_d) = \dot{x} + (x - x_d) \tag{16}$$

where x_d is the target location in the insertion frame. Furthermore, owing to the tissue deformation and the target movement x_d is a function of time.

Here as $s \to 0$ it can be deduced that $\dot{x} \to 0$ and $x \to x_d$.

It is common in the sliding mode, to introduce a control signal u_{eq}, which satisfies the system dynamics of $\dot{s} = 0$

$$u_{eq} = -\left(\frac{\partial s}{\partial \chi}B\right)^{-1}\left(\frac{\partial s}{\partial \chi}f(\chi, t)\right) \tag{17}$$

Here u_{eq} is computed according to the formulation of the needle dynamics in the state space as follows

$$\chi = \begin{bmatrix}x_1\\ x_2\end{bmatrix}$$

$$\frac{\partial s}{\partial \chi} = [1 \;\; 1] \Rightarrow \frac{\partial s}{\partial \chi}B = \frac{1}{M_n}$$

$$\begin{aligned}u_{eq} &= -\left(\frac{\partial s}{\partial \chi}B\right)^{-1}\left(\frac{\partial s}{\partial \chi}f(\chi, t)\right)\\ &= -M_n x_2 + \varphi_v(x_1, x_2, w, \dot{w}, \ddot{w})\Theta\\ &= -M_n\dot{x} + \varphi_v(x, \dot{x}, w, \dot{w}, \ddot{w})\Theta\end{aligned} \tag{18}$$

If the soft tissue parameters are available, the inverse dynamics can be used to control the needle in the soft tissue.

We add terms to the u_{eq} computed by the sliding mode approach in the previous section and the control law proceeds as follows

$$\begin{aligned}u = u_{eq} - Gs + M_n\dot{x}_d = -M_n\dot{x} + \varphi_v(x, \dot{x}, w, \dot{w}, \ddot{w})\Theta\\ - Gs + M_n\dot{x}_d\end{aligned} \tag{19}$$

where $G > 0$ is a gain to be set by the designer of the controller system.

By substituting the u in (14) the closed-loop equation becomes

$$\begin{aligned}M_n\ddot{x} + \varphi_v(x, \dot{x}, w, \dot{w}, \ddot{w})\Theta = -M_n\dot{x} + \varphi_v(x, \dot{x}, w, \dot{w}, \ddot{w})\Theta\\ - Gs + M_n\dot{x}_d\end{aligned} \tag{20}$$

Since

$$\dot{s} = \ddot{x} + \dot{x} - \dot{x}_d \tag{21}$$

The closed-loop simplifies to

$$M_n\dot{s} + Gs = 0 \tag{22}$$

As the non-linear term of the dynamics equation is omitted through the usage of the inverse dynamics approach, it is easy to show that the system is closed-loop stable. Hence by choosing the classic Lyapunov function and derivation of this function along the closed-loop system trajectories it can be written

$$V = \frac{1}{2}M_n s^2 \Rightarrow \dot{V} = M_n\dot{s}s = -Gs^2 \leq 0 \tag{23}$$

Since V is radially unbounded, it can be deduced that the closed-loop system is globally stable. The proof of asymptotical stability is achieved using Barbălat lemma [38].

2.5 Robust control

In practice, the values of the tissue parameters are not exactly known, so owing to the arisen uncertainty, the

$$\operatorname{sign}(\dot{x})\sum_{a=1}^{n(x)}\sum_{b=1}^{l(a)}\vec{v}^{\mathrm{T}}\cdot(M_{ab}\ddot{w}_b + C_{ab}\dot{w}_b + K_{ab}w_b) = \operatorname{sign}(\dot{x})\sum_{a=1}^{n(x)}\sum_{b=1}^{l(a)}\vec{v}^{\mathrm{T}}\cdot y_{ab}(w_b, \dot{w}_b, \ddot{w}_b)\Theta = \vec{v}^{\mathrm{T}}\cdot\varphi_v(x, \dot{x}, w, \dot{w}, \ddot{w})\Theta$$

$$y_{ab}(w_b, \dot{w}_b, \ddot{w}_b)$$

$$= \begin{bmatrix} w_{y_b}\beta_b\alpha_a + w_{x_b}\alpha_a\alpha_b & w_{y_b}\beta_a\alpha_b + 2w_{x_b}\alpha_a\alpha_b + w_{x_b}\beta_a\beta_b & \dot{w}_{xb}\alpha_a\alpha_b + \dot{w}_{yb}\beta_b\alpha_a & \dot{w}_{xb}\beta_a\beta_b + 2\dot{w}_{xb}\alpha_a\alpha_b + \dot{w}_{yb}\beta_a\alpha_b\dfrac{\ddot{w}_{xb}}{3}\dfrac{\ddot{w}_{xb}}{3}\\ w_{x_b}\beta_a\alpha_b + w_{y_b}\beta_a\beta_b & w_{x_b}\beta_b\alpha_a + 2w_{y_b}\beta_a\beta_b + w_{y_b}\alpha_a\alpha_b & \dot{w}_{yb}\beta_a\beta_b + \dot{w}_{xb}\beta_a\alpha_b & \dot{w}_{yb}\alpha_a\alpha_b + 2\dot{w}_{yb}\beta_a\beta_b + \dot{w}_{xb}\beta_b\alpha_a\dfrac{\dot{w}_{yb}}{3}\dfrac{\dot{w}_{yb}}{3}\end{bmatrix}$$

$$\varphi(x, \dot{x}, w, \dot{w}, \ddot{w}) = \operatorname{sign}(\dot{x})\sum_{a=1}^{n(x)}\sum_{b=1}^{l(a)}y_{ab}(w_b, \dot{w}_b, \ddot{w}_b) \tag{13}$$

inverse dynamics method proposed in the previous section may only be asymptotically stable for certain values of gain.

By denoting the estimation of the tissue parameters as $\hat{\Theta}$, the control signal in (19) can be restated

$$u = -M_n\dot{x} + \varphi_v(x, \dot{x}, w, \dot{w}, \ddot{w})\hat{\Theta} - Gs + M_n\dot{x}_d \tag{24}$$

and the closed-loop system will be

$$M_n\dot{s} + Gs = \varphi_v(x, \dot{x}, w, \dot{w}, \ddot{w})\tilde{\Theta} \tag{25}$$

where $\tilde{\Theta} = \hat{\Theta} - \Theta$. The Lyapunov function of (23) results in

$$\dot{V} = -Gs^2 + s\varphi_v(x, \dot{x}, w, \dot{w}, \ddot{w})\tilde{\Theta} \tag{26}$$

and the stability of the system cannot be deduced, however increasing the gain can lessen the effect of the second term in (26) and asymptotically stabilises the system.

The robust control law can be designed as

$$u = -M_n\dot{x} + \varphi_v(x, \dot{x}, w, \dot{w}, \ddot{w})\hat{\Theta} - Gs + M_n\dot{x}_d \operatorname{sign}(s)\text{Ø}(x, \dot{x}, w, \dot{w}, \ddot{w}, \tilde{\Theta}) \tag{27}$$

where Ø(.) denotes the upper bound of the uncertainty term $(\varphi_v(.)\tilde{\Theta})$ in (25). By choosing the Lyapunov function in (23) it can be written

$$\dot{V} = -Gs^2 + s\varphi_v(x, \dot{x}, w, \dot{w}, \ddot{w})\tilde{\Theta} - \operatorname{sign}(s)s\text{Ø}(x, \dot{x}, w, \dot{w}, \ddot{w}, \tilde{\Theta}) \leq 0 \tag{28}$$

and the global and asymptotical stability can be achieved the same as before.

However since the sign(.) function causes chattering in the system, it can be replaced by some smoother function such as function

$$u = -M_n\dot{x} + \varphi_v(x, \dot{x}, w, \dot{w}, \ddot{w})\hat{\Theta} - Gs + M_n\dot{x}_d - \tanh(\gamma s)\text{Ø}(x, \dot{x}, w, \dot{w}, \ddot{w}, \hat{\Theta}) \tag{29}$$

where γ determines the smoothness of the function.

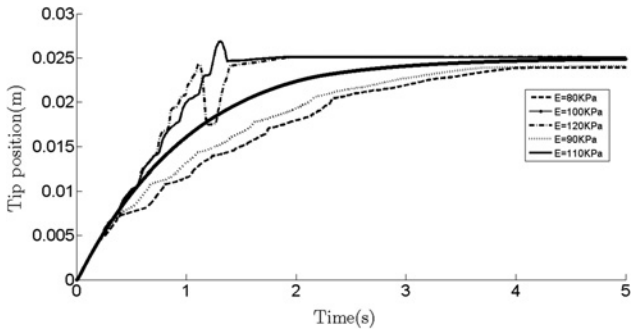

Fig. 3 *Needle tip position obtained by inverse dynamics for different values of Young modulus*

The upper bound of the uncertainty is determined by taking into account the maximum uncertainty on the tissue parameters $(\tilde{\Theta}_{max})$ as depicted in Table 1

$$\varphi_v(x, \dot{x}, w, \dot{w}, \ddot{w})\tilde{\Theta} \leq \text{Ø}(x, \dot{x}, w, \dot{w}, \ddot{w}, \tilde{\Theta}) = \varphi_v(x, \dot{x}, w, \dot{w}, \ddot{w})\tilde{\Theta}_{max} \tag{30}$$

3 Results

To inspect the various aspects of the proposed algorithm and to investigate the feasibility of the proposed methods, inverse dynamics control approaches is simulated. Inverse dynamics is utilised, with parameter uncertainty to demonstrate the system performance under inaccurate tissue mechanical parameter estimation. The needle–tissue model used in the simulations [28] employs the 2D and dynamic FEM as the model for tissue and the slip-stick as the needle–tissue contact model [17]. Furthermore per Table 1, in all simulation runs, the nominal tissue parameters (mean values) for Young modulus is assumed to be 100 kPa, which is the case for the CA; and Poisson ratio is assumed to be

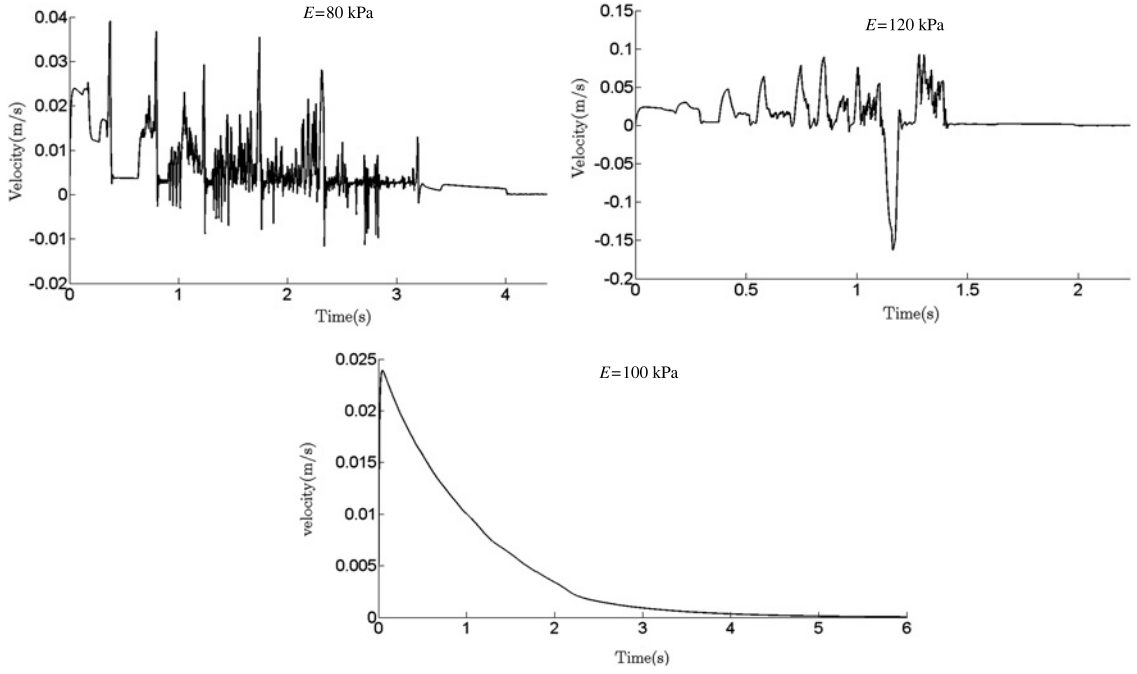

Fig. 4 *Needle velocity obtained by inverse dynamics for different values of Young modulus*

doi: 10.1049/iet-cta.2011.0449

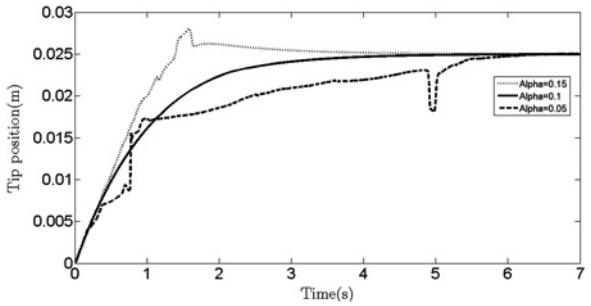

Fig. 5 *Needle-tip position obtained by inverse dynamics for different values of α*

0.490 to characterise the near incompressibility of the soft tissue behaviour. The nominal value for α is assumed to be 0.1 [33].

To simulate the cases with uncertainty in tissue parameter, different amounts of parameters were simulated. It was observed that the sensitivity to Poisson ratio is quite negligible. Also the sensitivity to the element mass is quite low, which results in the negligible role of β (in the Rayleigh damping equation) in the system performance. The uncertainty is assumed to be between 80 kPa and 120 kPa for Young modulus according to Table 1; and 0.05 and 0.15 for α.

The needle mass that includes the needle and the holder in the experimental setup is assumed to be 0.100 kg. The location of the target is assumed to be $[2.5\ 2.5]^T$ cm deep in the tissue in the world frame (x–y frame of Fig. 1) and the needle is always inserted in the x-direction of the world frame.

3.1 Inverse dynamics

3.1.1 Effect of parameter uncertainty: (a) Uncertainty only in Young modulus: To demonstrate the effect of the uncertainty in Young modulus estimation, the simulation was performed with $G = 10$ (which stabilises the system under uncertainty) and Poisson ratio of 0.490 and α of 0.1. As it is shown in Fig. 3 the response of the system alters from over-damped to under-damped for underestimation and overestimation of Young modulus, respectively. The underestimation of the Young modulus leads to a smaller

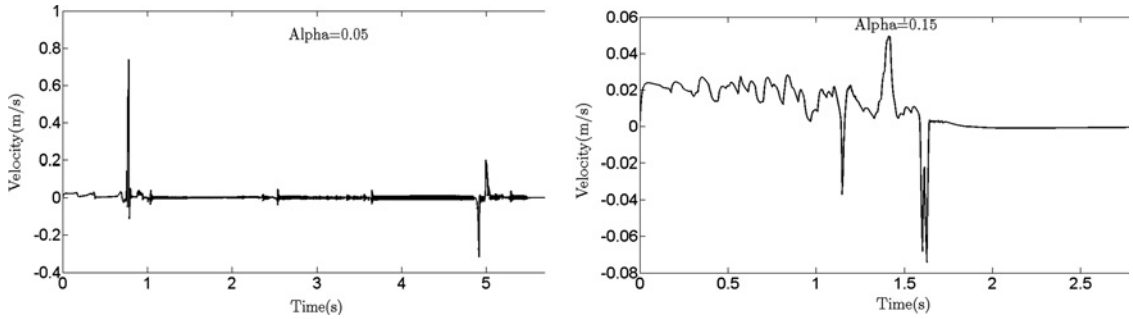

Fig. 6 *Needle velocity obtained by inverse dynamics for different values of α*

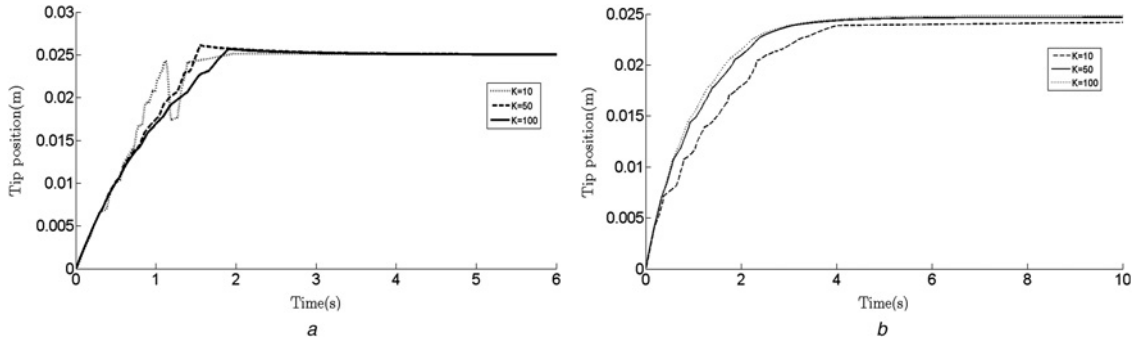

Fig. 7 *Needle-tip position obtained by inverse dynamics for different values of gain with Young moduli of*
a $E = 120$ kPa
b $E = 80$ kPa

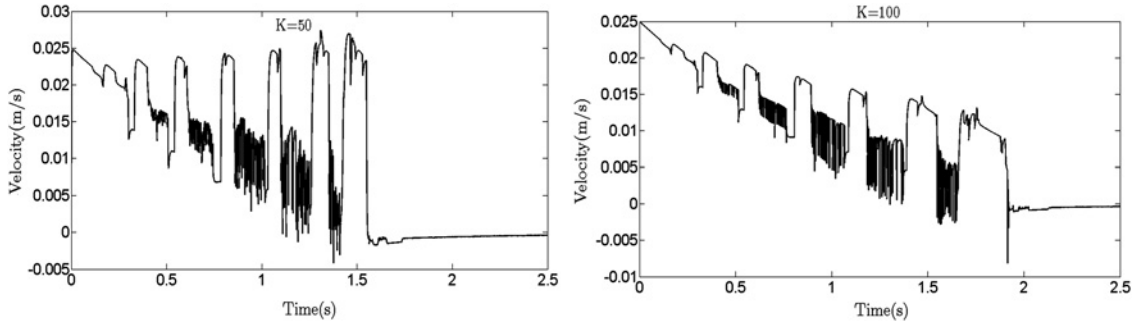

Fig. 8 *Needle velocity obtained by inverse dynamics for different values gain with Young modulus of $E = 120$ kPa*

control signal and hence a slower response, meanwhile overestimating the Young modulus leads to a larger control signal and hence the faster response will cause overshoot in the response. Overshoot in the response is undesirable as the needle could move beyond the desired target point, causing tissue damage and severe trauma.

Fig. 4 shows the velocity of the needle for various estimations of the Young modulus. The divergence form the nominal tissue Young modulus seems to have an undesirable effect on the velocity by decreasing the smoothness. Also in case of overestimation of Young modulus, the velocity is higher, which agrees with the fast response of Fig. 3.

(b) Uncertainty only in α (Rayleigh damping parameter): To investigate the effects of uncertainty for the estimation of α, the simulation was performed for different estimation of α with $G = 10$ and Young modulus of 100 kPa and Poisson ratio of 0.490.

Fig. 5 shows the needle tip position for different amounts of uncertainty in the estimation of α. These results suggest the uncertainty in the estimation of α resembles to that of the Young modulus, since according to (12), the elastic moduli are multiplied by this parameter.

Fig. 6 depicts the needle velocity for different estimations of α. Again, the divergence of the estimation from the nominal value seems to decrease the smoothness of the velocity.

3.1.2 Effect of the controller gain: Next, the effect of controller gain (G) is investigated on the performance of the system with the inverse dynamics control and parameter uncertainty.

Fig. 7 shows the needle tip position obtained by inverse dynamics method with uncertainty in Young modulus (80 and 120 kPa) and Poisson ratio of 0.490 and α of 0.1. As it can be seen the needle tip position further resembles the case with no uncertainty (bold curve of fig. 3) as the gain is increased, also as seen in Figs. 8 and 9, the velocity profile becomes smoother with smaller spike-like peaks.

Moreover as depicted in Figs. 10–12 increasing gain improves the position and velocity profile of the needle dramatically. Increasing the gain dominates the role of the error-based term of the control signal (Gs) and reduces the undesired effect of uncertainty in tissue properties (Θ).

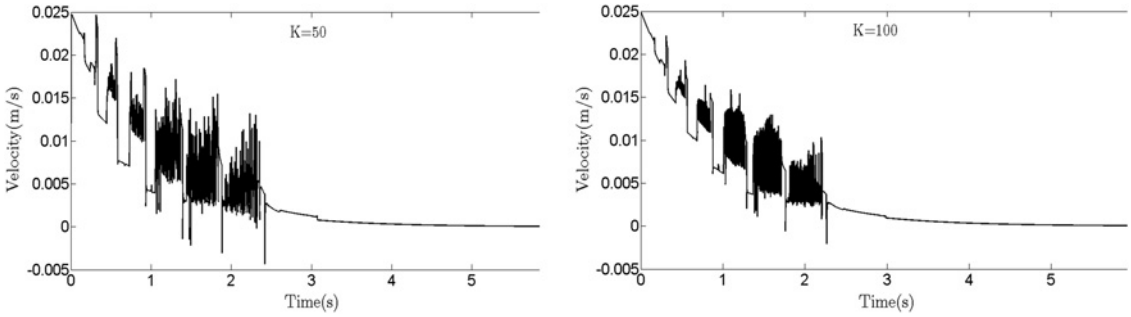

Fig. 9 *Needle velocity obtained by inverse dynamics for different values of gain with Young modulus of $E = 80$ kPa*

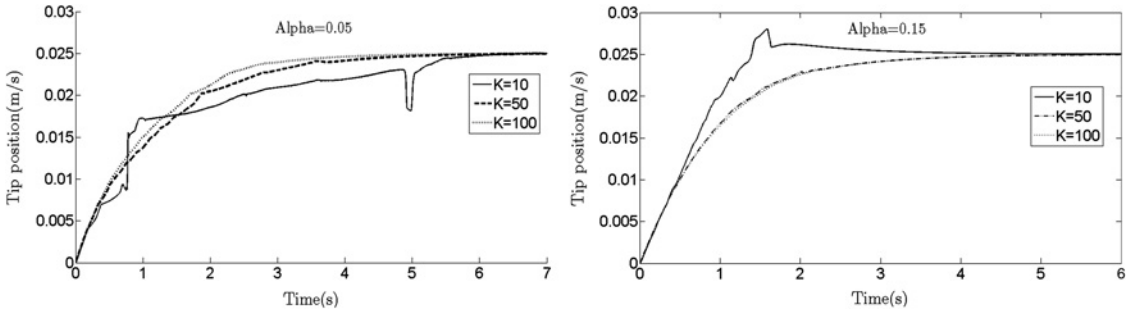

Fig. 10 *Needle tip position obtained by inverse dynamics for different values gain with α of*
a 0.05
b 0.15

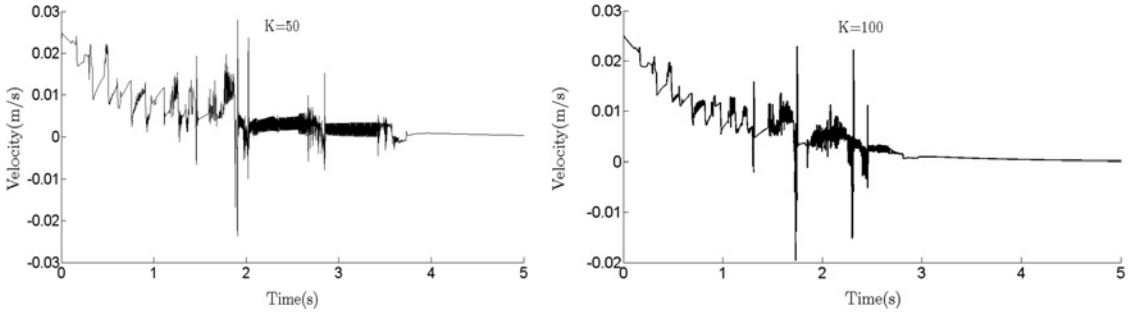

Fig. 11 *Needle velocity obtained by inverse dynamics for different values gain with α of 0.05*

doi: 10.1049/iet-cta.2011.0449

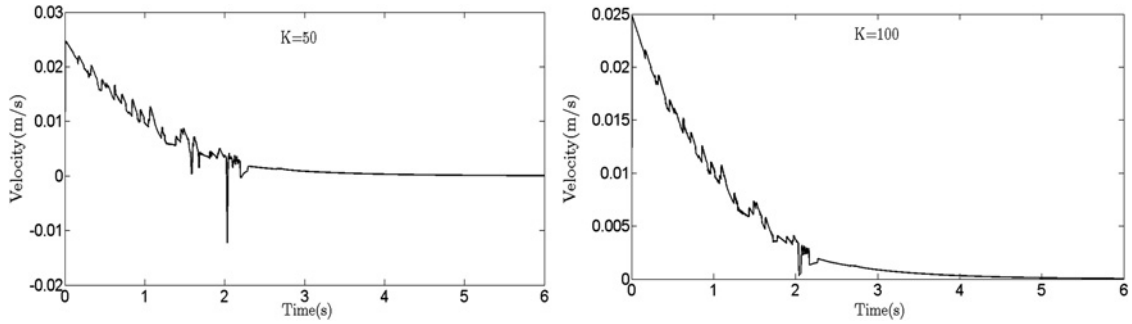

Fig. 12 *Needle velocity obtained by inverse dynamics for different values gain with α of 0.15*

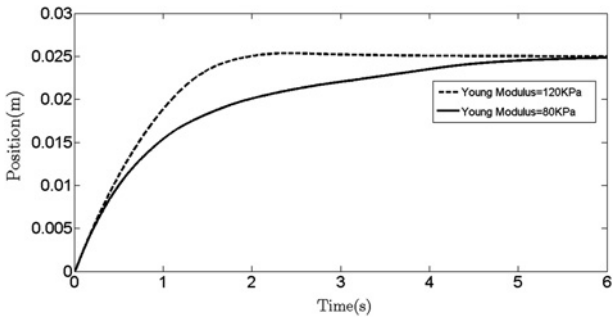

Fig. 13 *Needle-tip position obtained by robust controller with sign function for two different values of Young moduli*

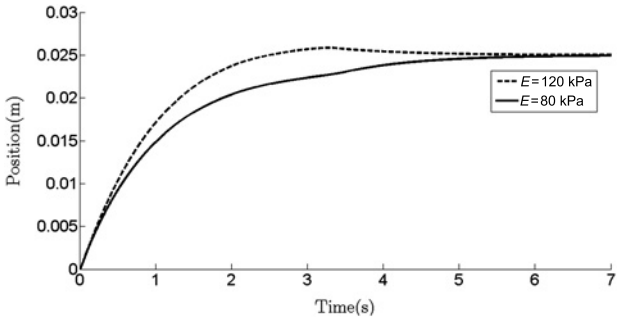

Fig. 15 *Needle tip position obtained by robust controller with tanh function for two different values of Young moduli*

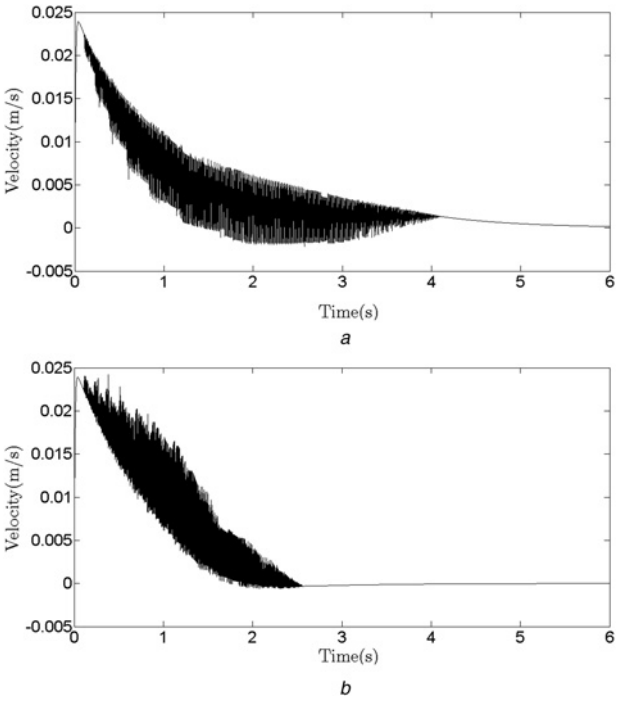

Fig. 14 *Needle velocity obtained by robust controller with sign function for two different values of Young moduli*

a 80 kPa
b 120 kPa

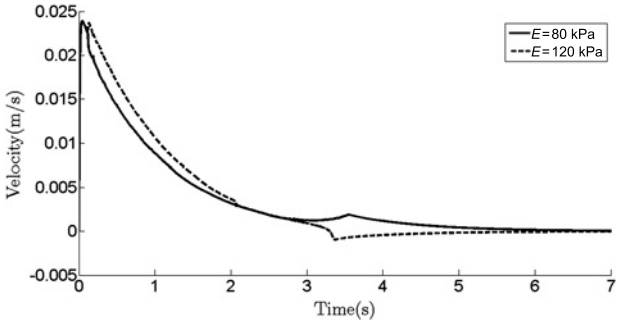

Fig. 16 *Needle velocity obtained by robust controller with tanh function for two different values of Young moduli*

3.2 Robust control

The robust controller proposed in Sections 2–5 was simulated under uncertainty in tissue parameters. For the sake of brevity, the uncertainty in Young modulus is only investigated here. In this case, according to Table 1, the value of $\tilde{\Theta}_{max}$ was calculated considering the maximum fluctuation of Young modulus of 40 kPa.

Figs. 13 and 14 show the needle tip position and velocity profile obtained by robust controller with sign function, for Young moduli of 80 and 120 kPa. As it was expected, the sign function causes chattering in the system. To reduce the chattering, next the robust controller with a smoother function is exploited.

Figs. 15 and 16 depict the needle tip position and needle velocity, respectively, obtained using the robust controller ($\gamma = 500$) with uncertainty in Young modulus and gain of 10. These results suggest a dramatic improvement of the system response; however, the overshoot in the case of overestimation of the Young modulus is still observable, but its amplitude is decreased significantly.

4 Discussion

The simulations endorsed the stability analysis discussed in the previous sections and the reaching error along the insertion direction always tends to zeros.

To address the role of tissue parameters in the needle control, the inverse dynamics method with uncertainty in the tissue parameters was investigated. For the uncertainty in Young modulus two types of degraded system responses were observed; the delayed and slow response owing to the underestimation of Young modulus and overshoot owing to the overestimation of Young modulus. This phenomenon can be explained by taking into account the control signal $\hat{\Theta}$ instead of Θ in (19). Recall that the control signal was the external driving force applied to the needle to direct it into the tissue. When the controller underestimated the Young modulus, the generated control signal was smaller as if it was being generated for a softer tissue, thereby resulting in a slower response. In contrary, when the controller overestimated the Young modulus, the generated control signal was larger because it was being generated for a stiffer tissue and thereby more force was needed to drive into the tissue and the result was overshooting the target. It was further shown that deviation from the nominal tissue Young modulus causes less smoothness and spikes in the needle velocity profile. The uncertainty in α parameter was also investigated and the system showed the same trend as the case with Young modulus uncertainty.

The role of the controller gain (G) was further investigated in the case of inverse dynamics with uncertainty in tissue parameters. It was seen that increasing the controller gain improved the needle tip position's profile by suppressing the overshoot in the case of Young modulus overestimation and improving the latency in the case of Young modulus underestimation. It was also observed that increasing controller gain decreased the smoothness of the velocity. The improvement in the response can be explained by separating the terms in the control signal in (12), into two categories; namely dynamics-based term of $\varphi_v(x, \dot{x}, w, \dot{w}, \ddot{w})\hat{\Theta}$ and kinematics-based terms. Increasing G accentuates the effect of the kinematics-based terms and reduces the effect of the dynamics-based term which contains the parameter mismatch.

Although high-gain approach increases the robustness of the system, owing to practical issues in its implementation such as actuator saturation, it may not be the best solution. Therefore a sliding mode robust controller was proposed and simulated. The result shows the improvement in system response, that is, more smooth velocity profile and less overshoot in the case of overestimation of the Young modulus and faster response in the case of underestimation of Young modulus.

5 Conclusion

This study considers a novel approach towards evaluation of controller design in driving a needle into prostate tissue. The proposed scheme introduced and simulated a model-based dynamics equation of the needle–tissue system. Inverse dynamics controllers were investigated in order to address the role of tissue parameter estimation in needle insertion problem and to highlight the role of different controller gains. It was shown that parametric mismatch owing to the uncertainty in the soft tissue's parameter can have drastic effects in the system behaviour. The robust controller approach improved the system response meaningfully as it benefits from the knowledge of the system model, upper bound of parameter uncertainty and the deformation data of the tissue.

6 References

1 Wei, Z., Wan, G., Gardi, L., Mills, G., Downey, D.: 'A Fenster, Robot-assisted 3D-TRUS guided prostate brachytherapy: system integration and validation', *Med Phys.*, 2004, **31**, (3), pp. 539–48

2 Danese, D., Sciacchitano, S., Farsetti, A., Andreoli, M., Pontecorvi, A.: 'Diagnostic accuracy of conventional versus sonography-guided fine-needle aspiration biopsy of thyroid nodules', *Thyroid*, 1998, **8**, (1), pp. 15–21

3 Rizun, P.R., McBeth, P.B., Louw, D.F., Sutherland, G.R.: 'Robot-assisted neurosurgery', *Semin. Laporasc. Surg.*, **2004**, **11**, (2), pp. 99–106.

4 Abolhassani, N., Patel, R., Moallem, M.: 'Needle insertion into soft tissue: A survey', *Med. Eng. Phys.*, 2007, **29**, (4), pp. 413–431

5 Alterovitz, R., Goldberg, K., Pouliot, J., Taschereau, R., Hsu, I.C.: 'Sensorless planning for medical needle insertion procedures'. Proc. IEEE/RSJ Int. Conf. on Intelligent Robots Systems, 2003, pp. 3337–3343

6 DiMaio, S.P., Salcudean, S.E.: 'Needle insertion modeling and simulation', *IEEE Trans. Robot. Autom: Spec. Issue Med. Robot*, 2003, **19**, (5), pp. 864–875

7 Alterovitz, R., Pouliot, J., Taschereau, R., Hsu, I.C., Goldberg, K.: 'Simulating needle insertion and radioactive seed implantation for prostate brachytherapy'. Proc. Medicine Meets Virtual Reality, 2003, pp. 19–25

8 Goksel, O., Salcudean, S.E., DiMaio, S. P.: '3D simulation of needle–tissue interaction with application to prostate brachytherapy', *Comput. Aided Surg.*, 2006, **11**, (6), pp. 279–288

9 Goksel, O., Salcudean, S.E., DiMaio, S.P., Rohling, R., Morris, J.: '3D needle–tissue interaction simulation for prostate brachytherapy'. Proc. Int. Conf. on Medical Image Computing and Computer Assisted Intervention, 2005, pp. 827–834

10 Dehghan, E., Salcudean, S.E.: 'Needle insertion point and orientation optimization in non-linear tissue with application to brachytherapy'. Proc. IEEE Int. Conf. Robotics and Automation, Roma, Italy, April 2007, pp. 2267–2272

11 Maurin, B., Barbe, L., Bayle, B., *et al.*: '*In vivo* study of forces during needle insertions'. Proc. Scientific Workshop on Medical Robotics, Navigation and Visualization (MRNV), Remagen, Germany, 2004, pp. 415–22

12 Simone, C., Okamura, A.M.: 'Modeling of needle insertion forces for robot-assisted percutaneous therapy'. Proc. IEEE Int. Conf. on Robotics and Automation (ICRA), Washington DC, USA, 2002, pp. 2085–91

13 Simone, C.: 'Modelling of needle insertion forces for percutaneous therapies', Master's thesis, Johns Hopkins University, 2002

14 Okamura, A.M.: 'Force modeling for needle insertion into soft tissue', *IEEE Trans. Biomed. Eng.*, 2004, **51**, (10), pp. 1707–16

15 Podder, T.K., Sherman, J., Clark, D.P., *et al.*: 'Evaluation of robotic needle insertion in conjunction with *in vivo* manual insertion in the operating room', Proc. IEEE Int. Workshop on Robot and Human Interactive Communication, Nashville, USA, 2005, pp. 66–72

16 Karnopp, D.: 'Computer simulation of stick-slip friction in mechanical dynamic systems', *Trans. ASME. J. Dyn. Syst. Meas. Control*, 1985, **107**, pp. 100–3

17 DiMaio, S.P., Salcudean, S.E.: 'Interactive simulation of needle insertion models', *IEEE Trans. Biomed. Eng.*, 2005, **52**, (7), pp. 1167–79

18 Crouch, J.R., Chad, M.S., Wainer, J., Okamura, A.M.: 'A velocity-dependent model for needle insertion in soft tissue'. MICCAI, CA, USA, 2005 (*LNCS* **8**), (2), pp. 624–32

19 Dehghan, E., Xu, W., Zahiri-Azar, R., Marchal, M., Salcudean, S.E.: 'Modeling of needle-tissue interaction using ultrasound-based motion estimation'. Proc. Int. Conf. Medical Image Computing and Computer-Assisted Intervention (MICCAI), Brisbane, Australia, 2007, pp. 709–716

20 DiMaio, S.P., Salcudean, S.E.: 'Needle steering and motion planning in soft tissues', *IEEE Trans. Biomed. Eng.*, 2005, **52**, (6), pp. 965–974

21 Alterovitz, R., Lim, A., Goldberg, K., Chirikjian, G.S., Okamura, A.M.: 'Steering flexible needles under Markov motion uncertainty'. Proc. IEEE/RSJ Int. Conf. on Intelligent Robots Systems, Edmonton, Alberta, Canada, 2005, pp. 1570–1575

doi: 10.1049/iet-cta.2011.0449

22 Alterovitz, R., Goldberg, K., Pouliot, J., Taschereau, R., Hsu, I.C.: 'Sensorless planning for medical needle insertion procedures'. Proc. IEEE/RSJ Int. Conf. on Intelligent Robots Systems, Las Vegas, USA, 2003, vol. **3**, pp. 3337–3343

23 Alterovitz, R., Goldberg, K., Okamura, A.: 'Planning for steerable bevel-tip needle insertion through 2D soft tissue with obstacles'. Proc. IEEE Int. Conf. on Robots. 2005, pp. 1640–1645

24 Webster, R.J., Kim, J.S., Cowan, N.J., Chirikjian, G.S., Okamura, A.M.: 'Nonholonomic modeling of needle steering', *Int. J. Robot. Res.*, 2006, **25**, (5/6), pp. 509–525

25 Park, W., Kim, J.S., Zhou, Y., Cowan, N.J., Okamura, A.M., Chirikjian, G.S.: "Diffusion-based motion planning for a nonholonomic flexible needle model'. Proc. IEEE Int. Conf. on Robots, 2005, pp. 4600–4605

26 Glozman, D., Shoham, M.: 'Flexible needle steering and optimal trajectory planning for percutaneous therapies'. Proc. Medical Image Computing Computer Assisted Intervention, New York, 2004, pp. 137–144

27 Dehghan, E., Salcudean, S.E.: 'Needle insertion parameter optimization for brachytherapy', *IEEE Trans. Robo.*, 2009, **25**, (2), pp. 303–315

28 Maghsoudi, A., Jahed, M.: 'Multi-parameter sensitivity analysis for guided needle insertion through soft tissue'. Proc. IEEE EMBS Conf. Biomedical Engineering & Sciences (IECBES), Kuala lampur, Malaysia, 2010, pp. 97–100

29 Ophir, J., Alam, S.K., Garra, B., *et al.*: 'Elastography: ultrasonic estimation and imaging of the elastic properties of tissues', *Inst. Mech. Eng., Part H: J. Eng. Med.*, 1999, **213**, (3), pp. 203–33

30 Jordán, P.: 'Image-based mechanical characterization of soft tissue using three dimensional ultrasound', PhD thesis, Harvard University, 2008

31 Slaughter, W.S.: 'The linearized theory of elasticity'. (Birkhauser, 2002)

32 Zienkiewicz, O.C., Taylor, R.L., Zhu, J.Z.: 'The finite element method: its basis and fundamentals'. (Elsevier Butterworth-Heinemann, 2005, 6th edn.)

33 McGarry, M.D.J.: 'Rayleigh damped magnetic resonance elastography'. Msc thesis, University of Canterbury, 2008

34 Hacksel, P.J., Salcudean, S.E.: 'Estimation of environment forces and rigid-body velocities using observers'. Proc. IEEE Int. Conf. Robotics, San Diego, CA, USA, 1994, pp. 931–936

35 Liu, C.S., Peng, H.: 'Disturbance observer based tracking control', *Trans. ASME*, 2000, **122**, (2), pp. 332–335

36 Yang, Z.J., Tsubakihara, H., Kanae, S., Wada, K., Su, C.Y.: 'A novel robust nonlinear motion controller with disturbance observer', *IEEE Trans. Control Syst. Technol.*, 2008, **16**, (1), pp. 137–147

37 Yu, X., Kaynak, O.: 'Sliding-mode control with soft computing: a survey', *IEEE Trans. Ind. Electron.*, 2009, **56**, (9), pp. 3275–3285

38 Khalil, H.K.: 'Nonlinear systems'. (Prentice-Hall, 2002, 3rd Edn.)